Science of the Total Environment 921 (2024) 171122

Contents lists available at ScienceDirect

Science of the Total Environment

journal homepage: www.elsevier.com/locate/scitotenv

Satellite-based aerosol optical depth estimates over the continental U.S. during the 2020 wildfire season: Roles of smoke and land cover

Jacob Daniels [a], Lu Liang [b,1], Katherine B. Benedict [c], Janice Brahney [d], Roman Rangel [b], Kathleen C. Weathers [e], Alexandra G. Ponette-González [f,g,*]

[a] Department of Electrical Engineering, University of North Texas, 1155 Union Circle #305279, Denton, TX 76203, USA
[b] Department of Geography and the Environment, University of North Texas, 1155 Union Circle #305279, Denton, TX 76203, USA
[c] Earth and Environmental Science Division, Los Alamos National Laboratory, P.O. Box 1663, Los Alamos, NM 87545, USA
[d] Department of Watershed Sciences and Ecology Center, Utah State University, 5210 Old Main Hill, Logan, UT 84322, USA
[e] Cary Institute of Ecosystem Studies, Box AB, Millbrook, New York 12545, USA
[f] Natural History Museum of Utah, University of Utah, 301 Wakara Way, Salt Lake City, UT 84108, USA
[g] Department of City and Metropolitan Planning, University of Utah, 375 South 1530 East, Suite 220, Salt Lake City, UT 84112, USA

HIGHLIGHTS

- Unprecedented wildfires have increased smoke density and aerosol pollution.
- MAIAC provides robust estimates of AOD under medium and high smoke density.
- MAIAC under- and overestimates AOD under mixed and smoke aerosol, respectively.
- MAIAC overestimates ground-based AOD most over barren land.

GRAPHICAL ABSTRACT

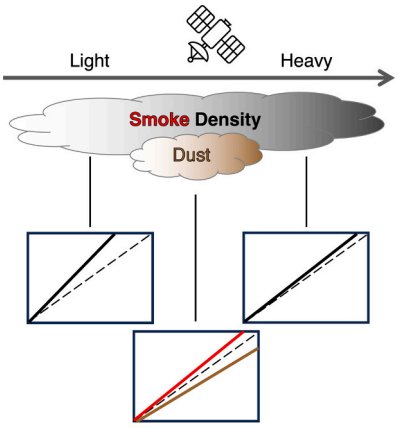

ARTICLE INFO

Editor: Philip Hopke

Keywords:
AERONET
Air quality
Ångström exponent
Dust

ABSTRACT

Wildfires produce smoke that can affect an area >1000 times the burn extent, with far-reaching human health, ecologic, and economic impacts. Accurately estimating aerosol load within smoke plumes is therefore crucial for understanding and mitigating these impacts. We evaluated the effectiveness of the latest Collection 6.1 MODIS Multi-Angle Implementation of Atmospheric Correction (MAIAC) algorithm in estimating aerosol optical depth (AOD) across the U.S. during the historic 2020 wildfire season. We compared satellite-based MAIAC AOD to ground-based AERONET AOD measurements during no-, light-, medium-, and heavy-smoke conditions identified

* Corresponding author at: Natural History Museum of Utah, University of Utah, 301 Wakara Way, Salt Lake City, UT 84108, USA.
E-mail address: alexandra.ponette@utah.edu (A.G. Ponette-González).
[1] Present address: Department of Landscape Architecture and Environmental Planning, University of California, Berkeley, 230 Bauer Wurster Hall #1820, Berkeley, CA 94720-1820, USA.

https://doi.org/10.1016/j.scitotenv.2024.171122
Received 25 August 2023; Received in revised form 16 February 2024; Accepted 18 February 2024
Available online 22 February 2024

MODIS
Particulate matter
Wildland-urban interface

using the Hazard Mapping System Fire and Smoke Product. This smoke product consists of maximum extent smoke polygons digitized by analysts using visible band imagery and classified according to smoke density. We also examined the strength of the correlations between satellite- and ground-based AOD for major land cover types under various smoke density levels. MAIAC performed well in estimating AOD during smoke-affected conditions. Correlations between MAIAC and AERONET AOD were strong for medium- ($r = 0.91$) and heavy-smoke ($r = 0.90$) density, and MAIAC estimates of AOD showed little bias relative to ground-based AERONET measurements (normalized mean bias = 3 % for medium, 5 % for heavy smoke). During two high AOD, heavy smoke episodes, MAIAC underestimated ground-based AERONET AOD under mixed aerosol (i.e., smoke and dust; median bias = −0.08) and overestimated AOD under smoke-dominated (median bias = 0.02) aerosol. MAIAC most overestimated ground-based AERONET AOD over barren land (mean NMB = 48 %). Our findings indicate that MODIS MAIAC can provide robust estimates of AOD as smoke density increases in coming years. Increased frequency of mixed aerosol and expansion of developed land could affect the performance of the MAIAC algorithm in the future, however, with implications for evaluating wildfire-associated health and welfare effects and air quality standards.

1. Introduction

Driven by the compounding effects of climate change and human activity, wildfires are increasing in frequency and intensity across many regions of the globe (Abatzoglou and Williams, 2016; Dennison et al., 2014; Ellis et al., 2022; Jones et al., 2022). In the continental U.S., recent wildfires have exposed millions of people to toxic smoke (Burke et al., 2021; Childs et al., 2022; Peterson et al., 2021) and have had profound impacts on terrestrial and aquatic environments (e.g., McKendry et al., 2019; Olson et al., 2023; Scordo et al., 2021). Close monitoring of the timing, location, and spatial extent of wildfire smoke is thus critical to determine the short- and long-term effects of smoke on human health (Chen et al., 2021; Holloway et al., 2021; Roberts and Wooster, 2021) and to better understand smoke risks to socio-ecological systems (e.g., Geng et al., 2018; Ponette-González et al., 2016).

Satellite earth observation products can provide continuous, consistent, and timely information on wildfire activity (Wooster et al., 2021) and associated smoke plumes, including their spatial and temporal distribution, source, and thickness (e.g., Bian et al., 2020; Brey et al., 2018; Filonchyk et al., 2022; O'Dell et al., 2020; Vadrevu et al., 2011). One such remote sensing-derived product extensively utilized in wildfire impacts research is aerosol optical depth (AOD). AOD provides a quantitative estimate of the amount of aerosol in the atmosphere and an efficient means to detect and characterize wildfire smoke over large geographic areas. Generally speaking, AOD values (at ~400–800 nm) can be used to indicate atmospheric conditions ranging from relatively clear with greater transmission of radiation (i.e., AOD < 0.2) to hazy with elevated aerosol concentrations and more light extinction (i.e., AOD > 0.6) (Martins et al., 2017). However, the accuracy and robustness of satellite-based AOD estimations depends on land surface characteristics (e.g., Falah et al., 2021; Loría-Salazar et al., 2016), atmospheric conditions (e.g., Tao et al., 2017), and assumptions in the algorithms regarding aerosol optical properties and ground surface reflectance (Falah et al., 2021). As such, changes in smoke density, composition, and distribution may not be accurately reflected in satellite-based AOD estimates, especially in the future as these characteristics change, with implications for models that use AOD to predict smoke impacts on air quality (Li et al., 2020b), agricultural productivity (Corwin et al., 2022), solar power production (Juliano et al., 2022), and climate (Tosca et al., 2013).

Given these implications, we used data from the historic 2020 U.S. wildfire season (1 July to 31 October 2020) to evaluate the utility of the Moderate Resolution Imaging Spectroradiometer (MODIS) Multi-Angle Implementation of Atmospheric Correction (MAIAC) AOD product across the continental U.S. in a more fire- and smoke-prone future. We compared satellite-based MAIAC AOD retrievals with ground-based AOD measurements from the Aerosol Robotic Network (AERONET) under varying smoke density levels (none, light, medium, heavy). We selected MAIAC AOD over other AOD products for three reasons. First, the MAIAC algorithm uses a "smoke test" to discriminate smoke from clouds (Lyapustin et al., 2012), increasing the amount of valid AOD observations during fire periods. Second, MAIAC AOD is widely used in smoke and modeling studies in the U.S. and other regions (e.g., Aguilera et al., 2021; Filonchyk et al., 2022; Li et al., 2020b; Loría-Salazar et al., 2021; Nguyen and Wooster, 2020). Third, compared to previous algorithms, such as Dark Target and Deep Blue, MAIAC provides more refined aerosol characteristics and higher spatial resolution (Tao et al., 2019).

The historic 2020 fire season provides a unique test case to assess the application of MAIAC for retrieving AOD during extreme fire and smoke. Between 2010 and 2019, an average of 64,000 fires burned ~2.8 million hectares (ha) across the continental U.S. (National Interagency Fire Center, 2020a). In 2020 alone, ~59,000 fires burned ~4.1 million ha, ~50 % more than the 2010–2019 decadal average. Among these were four of the 12 largest fires in the historical record (Keeley and Syphard, 2021). In the U.S. West, 27 megafires (i.e., burning >40,500 ha) in Arizona, California, Colorado, Oregon, Washington, and Wyoming (National Interagency Fire Center, 2020b) produced massive smoke plumes (e.g., 18 August to 25 August 2020, 11 September to 23 September 2020), some of which lofted and mixed with dust (González-Olalla et al., 2024). Others spanned the entire continental U.S., spilling into Canada, Mexico, and neighboring oceans. By every measure, 2020 was a historic fire and smoke year (Safford et al., 2022).

Here we evaluate satellite-based AOD estimates during a period of historic, continent-wide wildfire smoke, under varying smoke density levels, and over major U.S. land cover types. Building on previous studies that have examined the sensitivity of AOD products to land cover (e.g., Falah et al., 2021; Martins et al., 2017; Shaylor et al., 2022) and aerosol type (Falah et al., 2022), this work uniquely extends knowledge through evaluation under varying smoke conditions. In addition, this work evaluates the latest Collection 6.1 of the MAIAC algorithm. We discuss the implications of our findings in the context of future wildfire scenarios in which smoke is expected to be thicker, dust more prevalent, and developed land more expansive.

2. Material and methods

2.1. Data product descriptions

MODIS has been providing global AOD data with high temporal resolution for over 20 years. The MCD19A2 data product offers daily 1-km resolution land AOD grids by combining measurements from MODIS sensors aboard NASA's Aqua and Terra satellites, which have a local equator crossing time of 01:30 pm and 10:30 am, respectively.

The product employs the MAIAC algorithm (Lyapustin et al., 2018), which utilizes MODIS data from the preceding four to 16 days to create a baseline image of the surface background using multiple viewing angles that result from daily variations in satellite orbit path. Time series analysis and advanced image processing techniques allow the algorithm to decouple the surface background from the atmospheric data and improve the accuracy of satellite-based AOD retrievals (Lyapustin and

Wang, 2018). In Collection 6.1, the MAIAC algorithm has known limitations (Lyapustin and Wang, 2022): (1) high sun zenith angles (>70°) are expected to reduce performance; (2) in desert regions, it generates persistent high AOD in areas with bright salt pans, leading to missing surface retrievals; and (3) near coastlines, there are likely to be frequent artifacts in cloud mask and surface bidirectional reflectance factor, while AOD values may be higher.

The MCD19A2 Science Dataset layers include blue band AOD at 470 nm and green band AOD at 550 nm. The 550 nm band was used in this study due to lower sensitivity to atmospheric interference and higher overall consistency (Ranjan et al., 2020). Two AOD Quality Assurance layers were employed to filter potential outlier retrievals to obtain the best quality data (Lyapustin and Wang, 2018): the cloud mask to identify clouds immediately over a given pixel and an adjacency mask to assess cloud presence in the surrounding pixels.

We acquired the MCD19A2 data for the continental U.S. from the Atmospheric Archive and Distribution System Distributed Active Archive Center, spanning 1 July to 31 October 2020. Data from each of the standard MODIS tiles are reported with a single timestamp. Each of the tile's MAIAC AOD measurements is reported independently and depends on the satellite's orbit overpass time (Terra or Aqua). We focused on this time period to minimize the effects associated with seasonal changes in land cover and to maximize our ability to analyze different smoke densities due to the prevalence and severity of large fires at this time. In 2020, approximately 40 % (~23,000) of all fires and ~70 % of all hectares burned (~2.9 million) occurred between July and October (National Interagency Fire Center, 2020a). In addition, the average fire size during the study period was two times larger compared to the average fire size for July to October 2000–2019. The spatial and temporal distribution of burned area in 2020 also differed from previous years. Burned area peaked in September, when fires burned 1.4 million ha of land, the most on record. Spatially, 40 % of all hectares burned in the U.S. were in California and > 80 % were spread across the U.S. West. Of the 50 largest fires in 2020, all but one (in Alaska) occurred in the U. S. West. Although fires were concentrated in the U.S. West, smoke distribution was nearly continent-wide, with much of the U.S. experiencing smoke frequencies ranging from 40 to 100 days (Fig. S1).

We used ground-based AERONET AOD (hereafter AERONET AOD), also for the period 1 July to 31 October 2020, as the validation dataset. AERONET is a global instrument network of sun photometers established by NASA and PHOTONS that collects ground-based measurements of aerosol optical properties at unevenly distributed locations but at a higher accuracy than satellite-based retrievals (Holben et al., 1998). For the visible and near-infrared wavelengths, the AOD uncertainty of the AERONET instrument is 0.01, while for ultraviolet wavelengths the uncertainty is 0.02; this low uncertainty makes AERONET an ideal validation data set for satellite remote sensing products (Eck et al., 1999; Giles et al., 2019; Holben et al., 1998). AERONET AOD values as high as 7 can be measured (Eck et al., 2019). There are 446 AERONET sites in the continental U.S. A total of 94 AERONET sites reporting valid data during the study period were included in this analysis (Table S1). These sites represent diverse land cover types and fire regimes (Fig. S2).

AERONET AOD data are collected every 15 min (Holben et al., 2018) with three levels of data available: Level 1 unscreened data, Level 1.5 cloud-screened and quality-controlled data, and Level 2.0 quality-assured data (https://aeronet.gsfc.nasa.gov/new_web/index.html). AERONET Version 3 Level 2 AOD data were used in this study (Giles et al., 2019). In addition to AOD, we used the Ångström exponent at 440–675 nm as a proxy for particle size (Eck et al., 1999). Aerosol size distributions dominated by coarse mode particles such as dust and seasalt generally have Ångström exponents <1, whereas aerosol distributions dominated by fine mode particles such as smoke and urban aerosol have values >1 and often closer to 2.

We used the Hazard Mapping System (HMS) Fire and Smoke Product to determine smoke-affected days during the study period and to provide a qualitative indicator of smoke density. Described in detail by Rolph et al. (2009) and Brey et al. (2018), HMS is an interactive tool developed by NOAA NESDIS to provide daily fire locations and smoke plumes across North America (https://www.ospo.noaa.gov/Products/land/hms.html#maps). The HMS relies on automated fire detections from the imagery of seven NOAA and NASA satellites; the spatial resolution of these observations ranges from 375 m to 2 km. Due to the error associated with automatic detections, trained analysts visually verify automated fire detections by comparing them with satellite images. False fire detections are removed, and undetected fires are added to the dataset.

Fire locations producing smoke are then used as the basis for smoke detection, which is conducted using visible band imagery primarily from Geostationary Operational Environmental Satellites (GOES) and occasionally from polar orbiting satellites. When smoke is identified, the analyst outlines the maximum aerial horizontal extent of smoke plumes. These smoke polygons provide information on smoke presence in the atmospheric column. Smoke plumes are then qualitatively classified into three density categories—light, medium, or heavy—based on approximate smoke thickness in the satellite imagery. Smoke detection using visible imagery is restricted to daylight hours (i.e., nighttime smoke detection is not possible) and detection can be limited by cloud cover (Rolph et al., 2009). In certain regions, it can also be challenging to distinguish between smoke and haze (Brey et al., 2018). Thus, the HMS smoke plume data represent a conservative (i.e., lower bound) estimate of smoke occurrence. Despite these caveats, the HMS Fire and Smoke Product has been shown to be useful for a variety of applications and is now widely used in research to track smoke plumes and as an indicator of smoke density (e.g. Buysse et al., 2019; Bian et al., 2020; Dang et al., 2022; O'Dell et al., 2019; Wen et al., 2023).

To delineate land cover, we used the National Land Cover Database (NLCD)—an operational land cover monitoring program providing land cover information for the U.S. that is updated every few years (https://www.mrlc.gov/data/nlcd-2016-land-cover-conus). Derived from Landsat imagery, the NLCD has 30-meter spatial resolution and is classified into eight Level I categories using a supervised classification approach: water, developed, barren, forest, shrubland, herbaceous, planted/cultivated, and wetlands (Homer et al., 2007). The Level I overall accuracy of the 2016 product is 90.6 % via a third-party accuracy assessment (Wickham et al., 2021).

2.2. AOD pre-processing and MAIAC-AERONET AOD spatio-temporal matching

To ensure consistency, we interpolated AERONET AOD data to a wavelength of 550 nm since original data were not provided at this wavelength. The closest available wavelengths were 440 nm, 532 nm, 551 nm, and 675 nm. The optimal wavelengths for interpolation were based on the number of available data points. There were fewer missing values for the 440 nm and 675 nm wavelengths. Thus, these wavelengths were selected for interpolation using the following equation:

$$\tau_{550nm} = \tau_{\lambda_0} * \left(\frac{\lambda}{\lambda_0}\right)^{-\alpha}$$

where τ_λ is the AOD at the target wavelength λ (550 nm), $\tau_{\lambda 0}$ is AOD at a reference wavelength λ_0 (440 nm), and α is the Ångström exponent at 440–675 nm provided by AERONET (Yang et al., 2018).

To compare MAIAC and AERONET AOD, we matched data as closely as possible in space and time (Fig. 1). MODIS satellite imagery was the limiting temporal factor given the lower measurement frequency (typically 3–5 times per day over the CONUS) of the sensors compared to AERONET (~15 min). The location of the AERONET site was the limiting spatial feature given that AERONET provides AOD measurements for discrete points across the continental U.S. while MAIAC provides retrievals over a much larger area. For the matchups, buffer zones centered on each AERONET site were created with radii of 500 m, 1 km, 17.5 km, and 27.5 km (Table S1). Both smaller and larger averaging

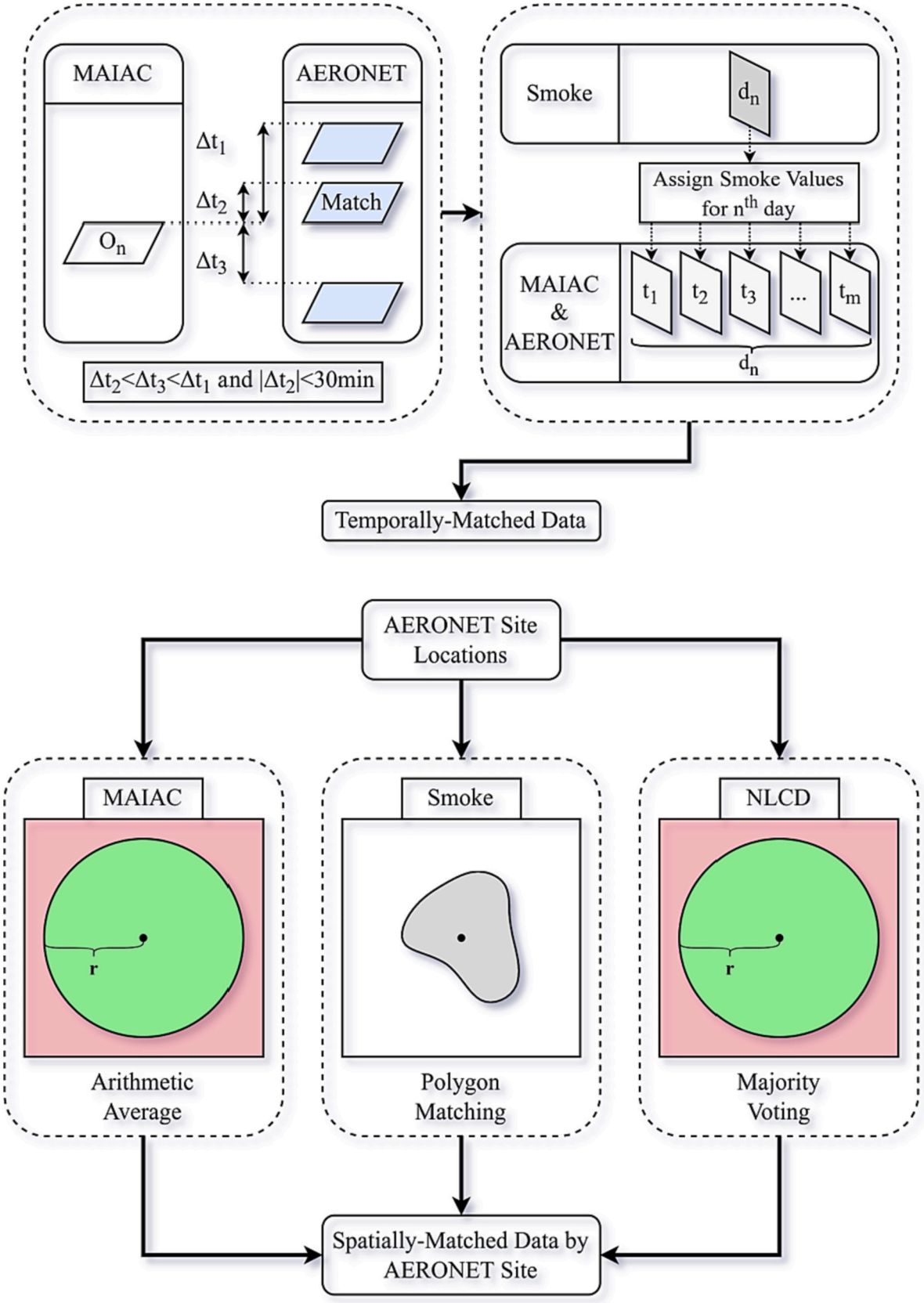

Fig. 1. Spatio-temporal matching procedure. The top panel describes the temporal matching of the data, and the bottom panel describes the spatial matching of the data. O_n is the satellite's nth orbit overpass time, Δt_x is the difference in measurement time between O_n and the nearest AERONET reporting times, d_n is the day *n* corresponding to any single day on which analysis occurred, and t_m is the mth orbit overpass time on day *n*, where m is the number of MODIS orbit overpass times for the current day *n*. r in the spatial matching is the buffer radius. Land cover was determined using 'majority voting' (i.e., the mode land cover within the buffer).

areas have been used in other validation studies of MAIAC and Deep Blue AOD products (Eibedingil et al., 2021; Falah et al., 2021; Petrenko et al., 2012; Shaylor et al., 2022; Superczynski et al., 2017).

Each MAIAC AOD measurement has an orbit overpass time which must be mapped to an AERONET AOD measurement on the ground. Therefore, for each orbit overpass time, the AERONET AOD measurement whose timestamp most closely matched that of the orbit overpass time was selected to provide a temporal match. If no AERONET AOD measurement existed within a ± 30-minute interval of the overpass time, the MAIAC measurement was discarded to reduce errors from AOD change over time (Eibedingil et al., 2021). For each of the temporal matches, MAIAC pixels were spatially matched to the most proximate AERONET site. To ensure a consistent, single timestamp within all given buffers, the AERONET sites with buffers overlapping multiple MODIS tiles were removed from the analysis.

Daily smoke polygons were temporally matched to the MAIAC-AERONET AOD matchups and spatially matched to each AERONET site. Since the frequency of MAIAC-AERONET AOD matchups was higher than that of the HMS polygons, there were instances when a single smoke polygon was assigned to multiple matchups to determine smoke density level for these matchups. For example, in cases with extensive smoke polygons and AERONET sites in close proximity, a single smoke polygon extended to cover multiple AERONET sites. Once a smoke polygon was assigned to a matchup time, smoke density (light, medium, heavy) was determined for each AERONET site. The NLCD data were also intersected with the MAIAC-AERONET AOD matchups.

2.3. Sensitivity analyses

A sensitivity analysis was conducted to examine how MAIAC AOD, averaged over different-sized sampling buffers around the AERONET sites (500 m, 1 km, 17.5 km, and 27.5 km; Table S1), would influence the relationship between MAIAC and AERONET AOD and to determine the optimal buffer size for spatial matching between the two AOD products. MAIAC pixels whose center fell within the buffer zones were averaged to obtain a single MAIAC AOD value for comparison with a single AERONET AOD value for that site, time, and buffer size. We examined changes in correlation coefficients between MAIAC and AERONET AOD with increasing buffer size.

We also examined the influence of land cover averaging area on relationships between MAIAC and AERONET AOD. For this analysis, we used sampling buffers with radii of 500 m, 1 km, and 10 km. We quantified the dominant land cover within the buffer zone around each AERONET site via majority voting (i.e., the mode land cover). Spatial matching was performed by assigning the dominant land cover type to each AERONET site.

The MAIAC AOD averaging area had a minimal effect on correlations between MAIAC and AERONET AOD at small buffer sizes (i.e., 500 m and 1 km radius), and this was consistent across smoke density levels (Fig. S3). However, at the larger buffer sizes of 17.5 km and 27.5 km, correlations between MAIAC and AERONET AOD generally decreased during light, medium, and heavy smoke density (Fig. S3). This general pattern held true regardless of land cover buffer size. Correlation coefficients between MAIAC and AERONET AOD also changed little with increasing land cover buffer size. Given these results, we selected a MAIAC AOD averaging area of 500 m around each AERONET site and a land cover averaging area of 500 m. Similar to Falah et al. (2021), we sought to take advantage of the high spatial resolution of the MAIAC AOD product, which captures fine-scale variability in aerosol and surface reflectance.

2.4. Statistical analysis

We used One-Way Analysis of Variance and Tukey's HSD post hoc tests to examine differences in mean AOD among smoke density levels and land cover types. To evaluate the relationship between MAIAC and AERONET AOD for varying smoke conditions and land cover types, we computed the Pearson correlation coefficient (r), which indicates the direction and the strength of the relationship between the two AOD measurement methods, and the normalized mean bias (NMB), which quantifies the average over- or under-prediction by MAIAC with respect to AERONET AOD. We used an expected error (*EE*) envelope to provide a visual and numerical representation of the acceptable range of error. Ideally, the EE envelope should contain ~68 % of the matchups (representing an accuracy of $\pm 1\sigma$) between satellite- and ground-based AOD (Levy et al., 2013). Here *EE*10 was calculated as

$$EE10 = \pm (0.05 + 0.10 * \mathrm{AOD}_{\mathrm{AERONET}})$$

after Falah et al. (2021). Finally, we examined the relationship between bias (MAIAC AOD - AERONET AOD) and the Ångström exponent to better understand the sensitivity of MAIAC AOD to particle size. All statistical analyses were performed in R. Significance was set at $p < 0.05$.

3. Results

3.1. AERONET AOD by smoke density level and land cover

Across all observations, AERONET AOD differed significantly by smoke density level. Mean AERONET AOD values were 3.2–8.5-fold higher during heavy- (mean = 0.77) compared to medium- (mean = 0.24), light- (mean = 0.13), and no-smoke- (mean = 0.09) conditions. For heavy smoke, the majority of AOD values were very high (i.e., first quartile = 0.27) relative to those for medium (first quartile = 0.12) and light (first quartile = 0.07) smoke. Maximum observed AERONET AOD was also considerably higher during heavy (4.49) than medium (2.45), light (1.81), and no smoke (0.53) (Table S2).

Within smoke density levels, there were marked variations in AERONET AOD among land cover types (Table S2). During heavy smoke, mean AERONET AOD ranged from 0.49 to 0.94 and was significantly higher over developed land (0.94) and shrubland (0.83) compared to all other land cover types. There was less variation among land cover types (range 0.21–0.26) under medium smoke, but planted/cultivated (0.26), shrubland (0.26), and developed land (0.25) exhibited higher mean AOD than herbaceous land (0.21). Similarly, under light smoke conditions, land cover differences in mean AERONET AOD were small (range 0.11–0.14) and showed the same general pattern (i.e., high AOD over planted/cultivated, shrubland, developed land and low AOD over herbaceous). AOD values during no-smoke conditions (0.07–0.11) were highest for developed and planted/cultivated land, lowest for shrubland, barren, and herbaceous land and intermediate for forests and wetlands. Developed land had the highest maximum AOD values under all smoke density levels: light (1.81), medium (2.45), and heavy (4.49). In contrast, maximum AOD was observed over forest land during smoke-free conditions.

3.2. MODIS MAIAC performance during smoke

During July to October 2020, sites affected by heavy smoke ($n = 63$) were concentrated in the western U.S. (Fig. 2). Compared to heavy smoke, medium smoke occurred more frequently at eastern and southern U.S. sites ($n = 82$). No-smoke conditions were prevalent at a larger number of sites ($n = 93$) as were light-smoke conditions ($n = 87$), and these sites were distributed across the continental U.S.

Overall, site-level correlation coefficients between MAIAC and AERONET AOD values for light, medium, and heavy smoke were much stronger than for no-smoke conditions (Table S3), with the Mountain West and California showing weak correlations during smoke-free conditions and strong correlations during smoke-affected conditions (Fig. 2). There was also less spatial variation in the strength of the correlations during smoke events compared to no-smoke conditions. The MODIS MAIAC algorithm overestimated AOD at several sites during no

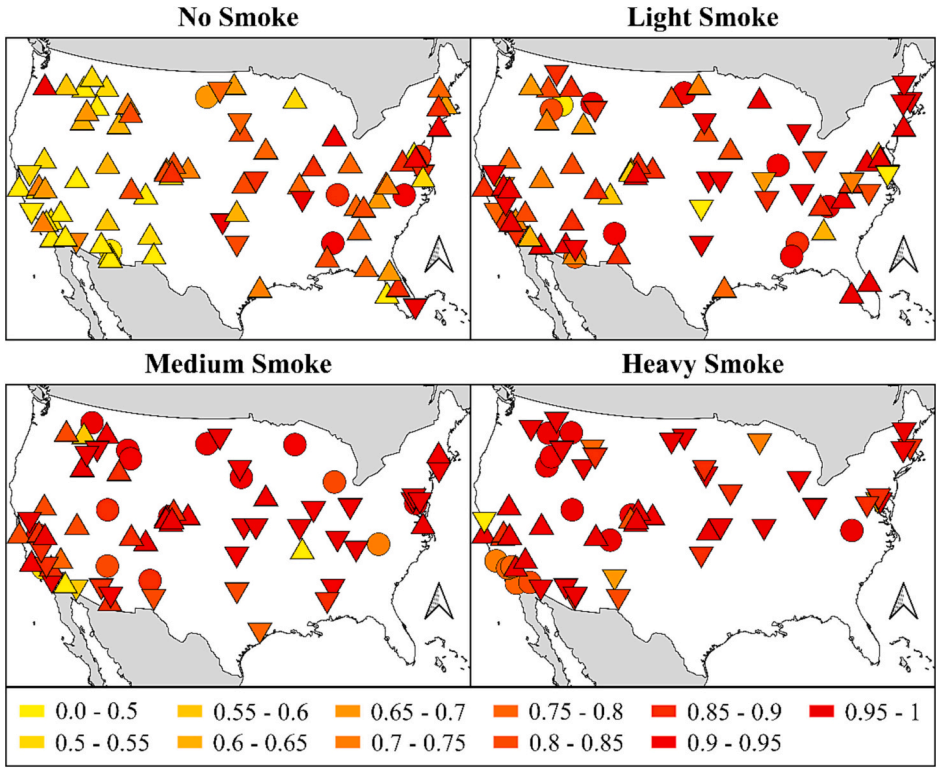

Fig. 2. Correlation coefficient and bias (unitless) between satellite-based (MAIAC) and ground-based (AERONET) observations of aerosol optical depth (AOD) during no smoke, light smoke, medium smoke, and heavy smoke across the continental U.S. for the study period (1 July to 31 October 2020) The color gradient shows the correlation coefficient (r) between MAIAC and AERONET AOD at the study sites. Upward-facing triangles indicate positive average normalized mean bias (NMB), downward-facing triangles indicate negative average NMB, and circles have an average NMB of no more than ±5 % across the study period.

smoke and underestimated AOD at more sites as smoke intensity increased (Fig. 2).

MODIS MAIAC overestimated AOD most during no-smoke conditions and overestimation decreased with increasing smoke density (Fig. 3). The correlation between satellite- and ground-based AOD was weakest for no smoke, and strongest for medium and heavy smoke density levels (Table S4).

3.3. Effect of particle size on MODIS MAIAC performance

During the study period, two heavy smoke events with high AOD peaks and contrasting Ångström exponents were identified (Fig. 4, top). The first, which spanned four days in mid-August (19 August to 22 August 2020) and encompassed 35 sites, had a mean MAIAC AOD of 0.76 and mean Ångström exponent of 1.73 (Fig. 4, middle). The second event occurred in mid-September (10 September to 12 September 2020) and affected 27 sites. Aerosol loading during the September event was higher (mean MAIAC AOD = 1.23), while the Ångström exponent was lower (mean = 1.1) than that of the August event. Differences in particle size between these events, as reflected in the Ångström exponents, were related to MAIAC AOD bias (Fig. 4, bottom). As Ångström exponents became smaller, MAIAC AOD showed increasing negative bias. Overall, MAIAC slightly overestimated AERONET AOD during the August event and underestimated AERONET AOD during the September event.

3.4. Interactions between smoke density and land cover on MODIS MAIAC performance

The correlation coefficient between satellite- and ground-based AOD was weakest while the magnitude of bias was greatest under smoke-free

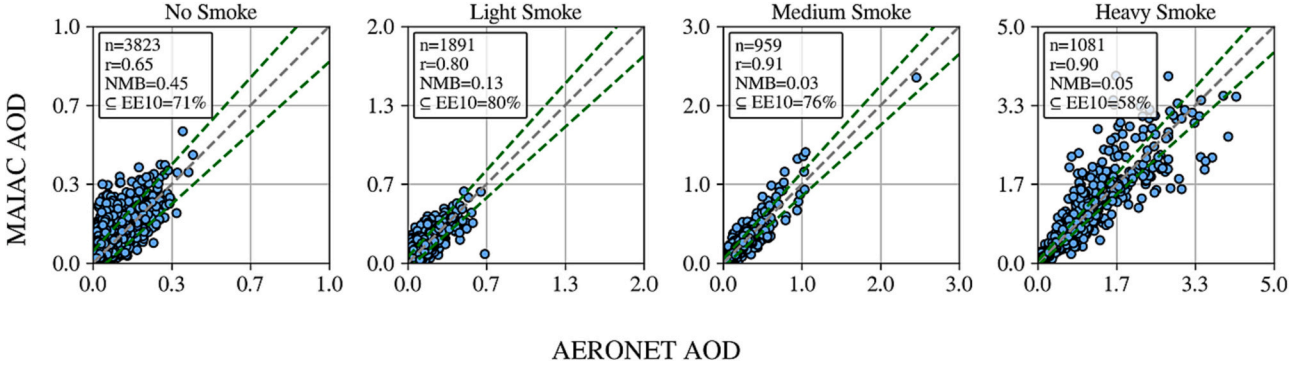

Fig. 3. Relationships between satellite- (MAIAC) and ground-based (AERONET) observations of aerosol optical depth (AOD) across smoke density levels for all matches across the study period (1 July to 31 October 2020). n is the number of data points, r is the correlation coefficient, NMB is the normalized mean bias, and *EE*10 is the expected error envelope.

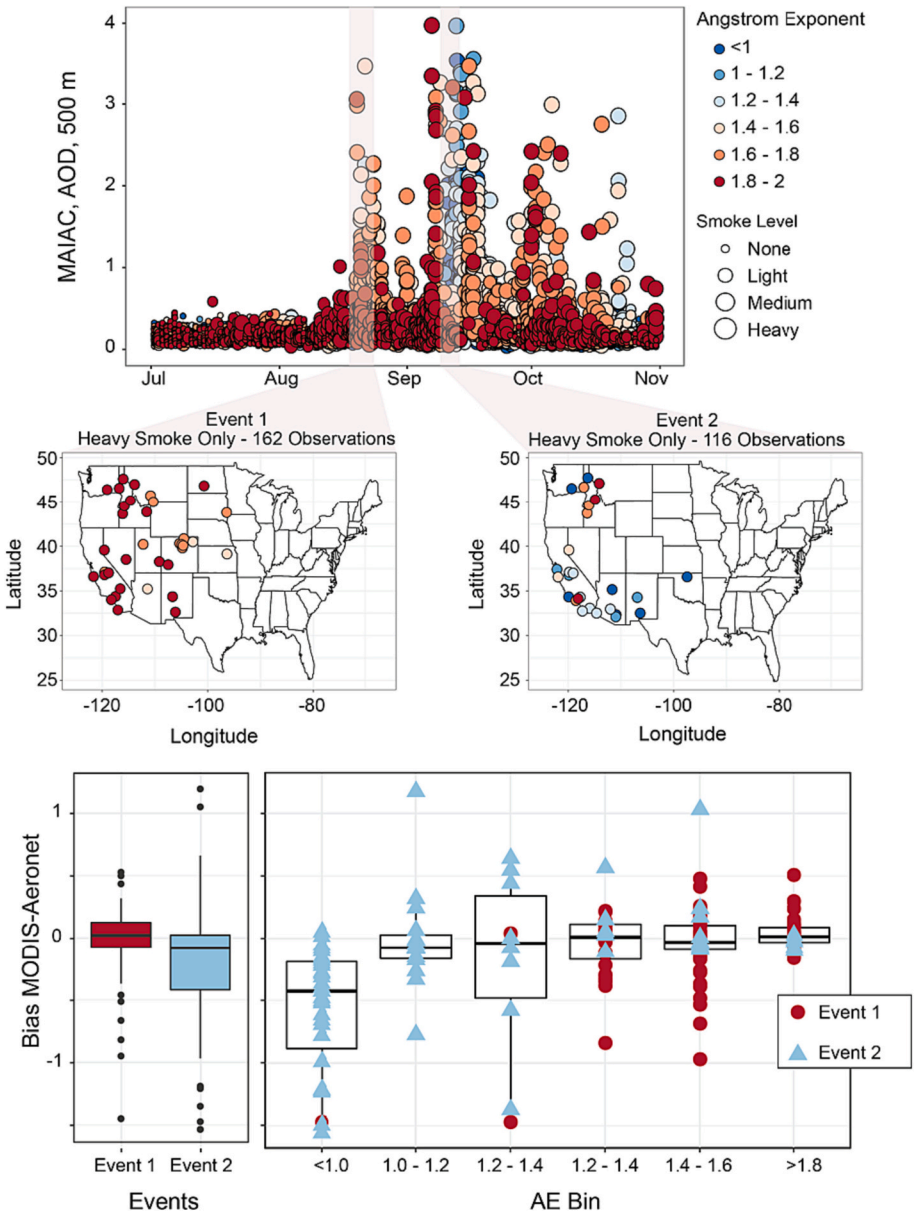

Fig. 4. The top panel shows a timeline of all MAIAC AOD values for all days between 1 July and 31 October 2020, and AERONET study sites in the continental U.S. Dot size is proportional to smoke density level, and color indicates the mean Ångström exponent value for each day. Grey bars indicate two high AOD heavy smoke events: 19 August to 22 August 2020 (Event 1) and 10 September to 12 September 2020 (Event 2). The middle panel shows only AERONET sites experiencing heavy smoke during the August and September heavy smoke events. Ångström exponent value for each site represents the average for each event. The bottom panel displays bias in satellite-based AOD (MAIAC AOD – AERONET AOD) by Ångström exponent values. Bottom left is the median bias for the August and September events.

conditions for all land cover types (Fig. 5). MODIS MAIAC overestimated AOD compared to AERONET AOD for all medium and heavy smoke-land cover combinations and, with few exceptions, the degree of overestimation became smaller as smoke density level increased (Fig. 5).

The MAIAC algorithm estimated AOD best over herbaceous and forest land cover across smoke density levels. Correlation coefficients between MAIAC and AERONET AOD were strong (Table S4), and the algorithm did not strongly over- or underestimate AOD. The strong performance of MAIAC over forest land cover was not surprising as forests—especially conifer forests—exhibit temporal stability, dark surfaces, and low background reflectance, which all lead to improved accuracy of AOD retrievals (e.g., Petrenko and Ichoku, 2013). Weaker correlations and higher levels of MAIAC AOD overestimation were seen for barren land under both light (NMB = 43 %) and medium smoke (NMB = 19 %). Under medium and heavy smoke, MAIAC was effective in estimating AERONET AOD over developed land: correlations between the products were strong and bias was small.

4. Discussion

4.1. Estimating AOD under worsening wildfire smoke

During the 2020 historic wildfire season, MAIAC performed very well in estimating AOD under all smoke density levels, especially under medium and heavy smoke when AERONET AOD reached values as high as 4.5. Previous versions of the algorithm were limited in the characterization of strong aerosol emissions causing MAIAC to underestimate AOD at high aerosol loading and for intense smoke plumes (Loría-Salazar et al., 2021; Lyapustin et al., 2018; Superczynski et al., 2017). Given the known underestimation of AOD for biomass burning aerosol

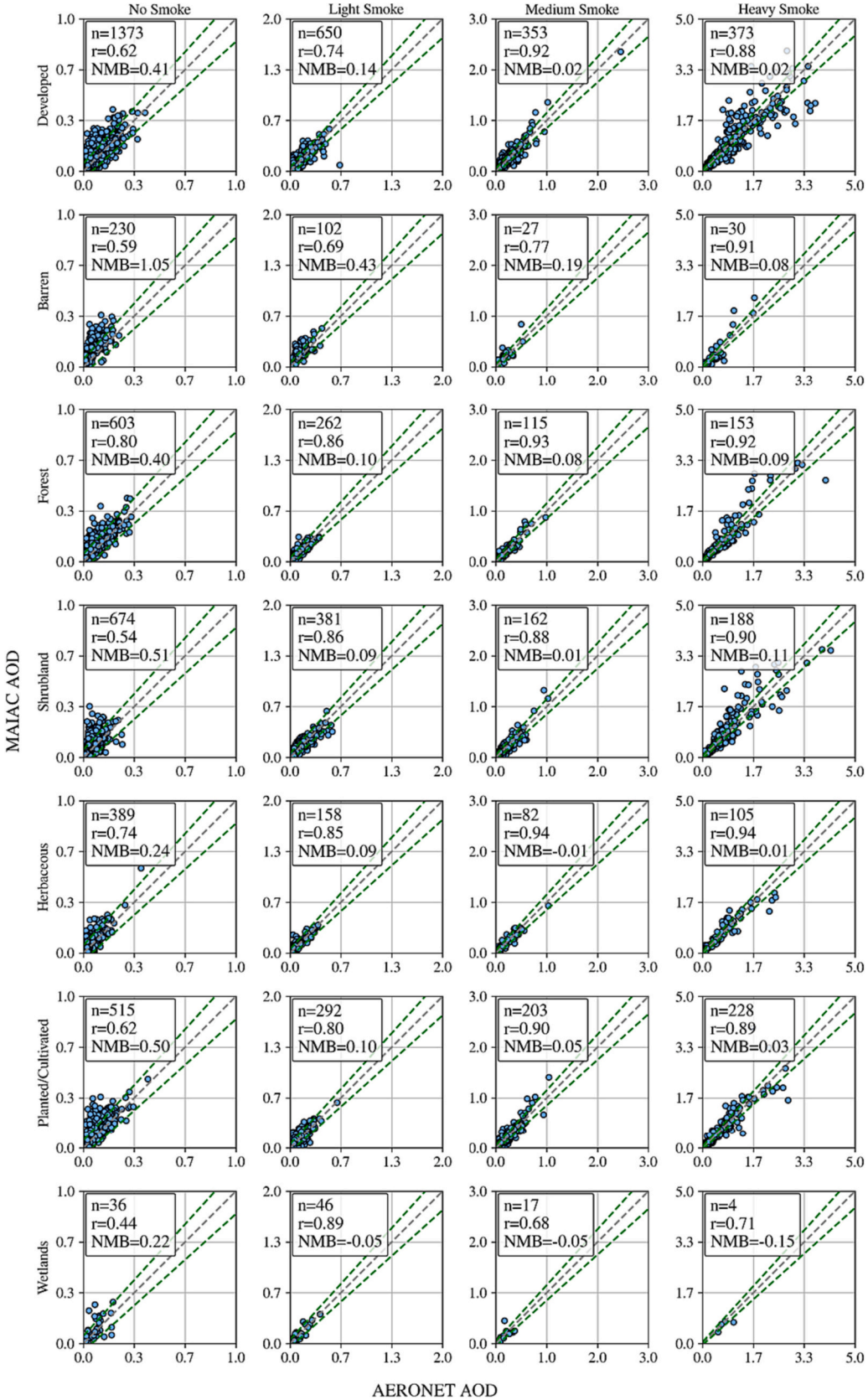

Fig. 5. Relationships between satellite-based (MAIAC) and ground-based (AERONET) observations of aerosol optical depth (AOD) across smoke density levels and land cover types for the period 1 July to 31 October 2020. n is the number of data points, r is the correlation coefficient, and NMB is the normalized mean bias.

during heavier smoke events, updates to the regional aerosol models were made in Collection 6.1 based on an analysis of AERONET data (Lyapustin and Wang, 2022). In addition, MAIAC C6.1 increased maximum AOD at 470 nm from 4 to 6.

In our analysis, we found strong correlations between MAIAC and AERONET AOD under medium and heavy smoke and a significant improvement in both overall bias and accuracy compared to Collection 6.0 (Fig. S4). Thus, our results confirm that updates to the MAIAC algorithm not only led to better AOD estimations under medium and heavy smoke but also demonstrate that these improvements are evident during a period of historic, continent-wide wildfire smoke.

Several characteristics of the fire and smoke events that occurred across the Western U.S. in 2020 could present challenges for the satellite retrieval of AOD in the future, however. Since the early 2000s, the number of smoke days across the U.S. has increased by approximately two days per year (Burke et al., 2021) and more of these smoke days are extreme (Wilmot et al., 2021). Intense fires can lead to exceptionally high AOD (Eck et al., 2023) and, under the most extreme conditions, can generate pyrocumulonimbus clouds that prevent AOD retrievals. Recent work suggests that there may be greater pyrocumulonimbus activity across various ecoregions in the western U.S. (Wilmot et al., 2022a). Furthermore, Eck et al. (2023) found that extreme forest fire events in the western U.S. were characterized by large variability in particle size and absorption properties. Such variability is a problem for satellite retrievals and regional aerosol models, which have difficulty with the complexity of smoke aerosol, particularly as it ages (Brown et al., 2021). In sum, in a more fire- and smoke-prone world, more extreme wildfire smoke and fire clouds could increase the uncertainty of satellite-based AOD retrievals.

4.2. Estimating AOD under co-occurring smoke and dust

Several record-breaking fires erupted in August and September 2020. The August Complex, the largest wildfire in California history, began in mid-August 2020 when thunderstorms and lightning associated with Tropical Storm Fausto triggered wildfires across the state (Cal Fire, 2020). The August Complex burned 418,000 ha and emitted large quantities of smoke and black carbon into the atmosphere, which then spread across the U.S. West (Patel, 2020). Consistent with high black carbon concentrations, 32 of 35 AERONET sites affected by heavy smoke between August 19–22 had Ångström exponents >1.6, indicating the dominance of fine-mode particles.

In mid-September, a cold front moving south from Canada generated high downslope winds along the mountains of Washington, Oregon, and California generating airborne dust while fueling existing fires and igniting new ones (Voiland, 2020). Wildfire smoke mixed with airborne dust forced road closures in Washington (White, 2020), while smoke and dust plumes were observed off the mountains in Oregon and Utah (Nelson, 2020). In California, firefighters faced concurrent threats of smoke and dust devils (Fedschun, 2020). During this period, 22 out of the 27 AERONET sites impacted by heavy smoke had Ångström values ≤1.2, indicating the influence of coarse mode aerosol and a mixed particle size distribution.

Smoke and dust can co-occur during fire events (Schlosser et al., 2017), driving differences in smoke properties among regions (Bian et al., 2020). Our analysis demonstrates that even during very heavy smoke, the MAIAC algorithm is sensitive to these differences. MAIAC overestimated AERONET AOD during the August smoke-dominated event and underestimated AERONET AOD during the September dust-affected smoke event. This finding is in line with the results of Falah et al. (2021) who, in a multi-region study, showed that periods of moderate to high aerosol loading dominated by coarse particles resulted in AOD underestimation by the MAIAC algorithm. Superczynski et al. (2017) also found greater bias in AOD retrievals during periods of high AOD with coarse or mixed particle sizes. Zhang et al. (2019) attributed large MAIAC AOD bias over desert regions to the algorithm's aerosol model. Should smoke and dust mixtures become more frequent as the scale and intensity of wildfires increase (Chauhan et al., 2018; Wagner et al., 2021), our findings suggest that this could affect the performance of the MAIAC algorithm.

4.3. Estimating AOD in developed areas and within the wildland-urban interface

While it is well known that the performance of the MAIAC algorithm is dependent on land cover (Falah et al., 2021; Martins et al., 2017; Shaylor et al., 2022), there are several reasons why the interface between developed and undeveloped land—the wildland-urban interface—in the western U.S. presents challenges for satellite-based AOD retrievals during smoke-affected periods. Between July and October 2020, mean and maximum AERONET AOD values over developed land across the continental U.S. were either the highest or among the highest under light, medium, and heavy smoke density levels. These high AOD values over developed land reflect a combination of local anthropogenic and transported smoke emissions. Notwithstanding, MAIAC was effective in estimating AERONET AOD over developed land during medium and heavy smoke: correlations between the two products were strong and normalized mean bias was small. These results differ with findings from previous evaluations of the Collection 6 MAIAC algorithm, which indicate that satellite retrievals are hampered over developed land by emissions from multiple pollution sources and the extensive and spatially varying coverage of bright surfaces (e.g., roads and buildings; Martins et al., 2017; Qin et al., 2021).

In contrast to developed land, satellite- and ground-based AOD were not as strongly correlated for barren land under the various smoke density levels, and there was considerable positive bias under light and medium smoke. The issue of bright surfaces affecting retrievals has been observed in other desert regions (but see Sever et al., 2017), where MAIAC has been found to overestimate AOD and result in a higher proportion of missing AOD values (Eibedingil et al., 2021; Li et al., 2020a; Qin et al., 2021; Zhang et al., 2019). The fact that many cities in the western U.S. are surrounded by desert complicates AOD retrievals in these areas (Li et al., 2020b; Loría-Salazar et al., 2016), and likely at their interface. Further expansion of developed land into undeveloped land will only increase the area over which satellite AOD retrievals can be difficult.

Fires that occur at the transition between developed and undeveloped land also generate emissions with distinct chemistries when compared with those of natural fuels (Jaffe et al., 2020). Coupled with the large number and concentration of emission sources in cities, smoke-affected developed areas are enveloped by increasingly complex aerosol mixtures. We and others (e.g., Rogozovsky et al., 2021; Superczynski et al., 2017) have shown that such mixtures are less well captured by the MAIAC algorithm and lead to underprediction of AOD.

While developed land continues to expand, recent estimates indicate that the wildland-urban interface now encompasses 5.6 %–18.8 % of the total land area across the conterminous U.S. (Carlson et al., 2022), including some 49 million residential homes (Burke et al., 2021). Fire prevalence in this transition zone heightens wildfire risk to communities and housing (Radeloff et al., 2018) and contributes to episodic AOD (and therefore particulate matter) spikes within cities (Filonchyk et al., 2022; Yang et al., 2021). As such, future research on satellite-based AOD estimates in the expanding transition zones between developed and neighboring areas during smoke periods is warranted.

5. Implications

Our research suggests that MAIAC provides robust estimates of AOD under worsening wildfire smoke, but that increased frequency of smoke-dust aerosol mixtures and expansion of developed land may affect the performance of the MAIAC algorithm. In a more fire- and smoke-prone future, accurately estimating AOD is crucial for developing robust

models of fine particulate matter, which rely on AOD as input data (Loría-Salazar et al., 2016). High-resolution estimates of near-surface air quality are critical both in the context of increasing population exposure to large fires (Peterson et al., 2021) and to the negative downwind effects of wildfire-emitted fine particulate matter—$PM_{2.5}$ (e.g., Buysse et al., 2019; Wilmot et al., 2022b). As smoke distributions increasingly overlap with population distributions (Peterson et al., 2021), accurate satellite-based AOD estimates will become ever more important for evaluating wildfire-associated health effects (Geng et al., 2018) and current air quality standards.

Declaration of generative AI in scientific writing

During the preparation of this work the authors did not use AI.

CRediT authorship contribution statement

Jacob Daniels: Writing – review & editing, Writing – original draft, Visualization, Investigation, Formal analysis, Data curation. **Lu Liang:** Writing – review & editing, Supervision, Resources, Methodology, Conceptualization. **Katherine B. Benedict:** Writing – review & editing, Visualization, Investigation. **Janice Brahney:** Writing – review & editing, Writing – original draft, Conceptualization. **Roman Rangel:** Investigation. **Kathleen C. Weathers:** Writing – review & editing, Conceptualization. **Alexandra G. Ponette-González:** Writing – review & editing, Writing – original draft, Visualization, Supervision, Investigation, Funding acquisition, Conceptualization.

Declaration of competing interest

The authors declare the following financial interests/personal relationships which may be considered as potential competing interests: Lu Liang reports financial support was provided by National Science Foundation.

Data availability

Data will be published at time of acceptance.

Acknowledgments

This research was supported by a University of North Texas Research Seed Grant and partially supported by NSF grant BCS-2117505 and Utah Agricultural Experiment Station UTA01669. The MCD19A2 version 6 MODIS datasets were obtained from the Atmospheric Archive and Distribution System (LAADS) Distributed Active Archive Center (DAAC). We acknowledge the MODIS mission scientists and associated NASA personnel for the production of the data used in this research effort. We also thank the AERONET PIs and their staff for establishing and maintaining the sites used in this investigation. We thank Phil Dennison for constructive feedback on our manuscript. We are grateful to four anonymous reviewers for their thoughtful feedback on this manuscript.

Appendix A. Supplementary data

Additional details are provided in the supporting information, including the number and spatial distribution of sites used in the analyses, AOD values under varying smoke densities and land cover types, correlations between satellite-based (MAIAC) and ground-based (AERONET) observations of aerosol optical depth (AOD) under various smoke density levels and land cover types, cumulative smoke distribution for the U.S. for 2020, and results of the sensitivity analysis. Supplementary data to this article can be found online at https://doi.org/10.1016/j.scitotenv.2024.171122.

References

Abatzoglou, J.T., Williams, A.P., 2016. Impact of anthropogenic climate change on wildfire across western US forests. Proc. Natl. Acad. Sci. 113, 11770–11775. https://doi.org/10.1073/pnas.1607171113.

Aguilera, R., Corringham, T., Gershunov, A., Benmarhnia, T., 2021. Wildfire smoke impacts respiratory health more than fine particles from other sources: observational evidence from Southern California. Nat. Commun. 12, 1493. https://doi.org/10.1038/s41467-021-21708-0.

Bian, Q., Ford, B., Pierce, J.R., Kreidenweis, S.M., 2020. A decadal climatology of chemical, physical, and optical properties of ambient smoke in the Western and Southeastern United States. J. Geophys. Res. Atmos. 125, e2019JD031372 https://doi.org/10.1029/2019JD031372.

Brey, S.J., Ruminski, M., Atwood, S.A., Fischer, E.V., 2018. Connecting smoke plumes to sources using Hazard Mapping System (HMS) smoke and fire location data over North America. Atmos. Chem. Phys. 18, 1745–1761. https://doi.org/10.5194/acp-18-1745-2018.

Brown, H., Liu, X., Pokhrel, R., Murphy, S., Lu, Z., Saleh, R., Mielonen, T., Kokkola, H., Bergman, T., Myhre, G., Skeie, R.B., 2021. Biomass burning aerosols in most climate models are too absorbing. Nat. Commun. 12 (1), 277. https://doi.org/10.1038/s41467-020-20482-9.

Burke, M., Driscoll, A., Heft-Neal, S., Xue, J., Burney, J., Wara, M., 2021. The changing risk and burden of wildfire in the United States. Proc. Natl. Acad. Sci. 118, e2011048118 https://doi.org/10.1073/pnas.2011048118.

Buysse, C.E., Kaulfus, A., Nair, U., Jaffe, D.A., 2019. Relationships between particulate matter, ozone, and nitrogen oxides during urban smoke events in the Western US. Environ. Sci. Technol. 53, 12519–12528. https://doi.org/10.1021/acs.est.9b05241.

Cal Fire, 2020. August Complex (includes Doe Fire) | CAL FIRE [WWW Document]. URL. https://www.fire.ca.gov/incidents/2020/8/16/august-complex-includes-doe-fire (accessed 6.28.23).

Carlson, A.R., Helmers, D.P., Hawbaker, T.J., Mockrin, M.H., Radeloff, V.C., 2022. The wildland–urban interface in the United States based on 125 million building locations. Ecol. Appl. 32, e2597 https://doi.org/10.1002/eap.2597.

Chauhan, A., de Azevedo, S.C., Singh, R.P., 2018. Pronounced changes in air quality, atmospheric and meteorological parameters, and strong mixing of smoke associated with a dust event over Bakersfield, California. Environ. Earth Sci. 77, 115. https://doi.org/10.1007/s12665-018-7311-z.

Chen, G., Guo, Y., Yue, X., Tong, S., Gasparrini, A., Bell, M.L., Armstrong, B., Schwartz, J., Jaakkola, J.J.K., Zanobetti, A., Lavigne, E., Saldiva, P.H.N., Kan, H., Royé, D., Milojevic, A., Overcenco, A., Urban, A., Schneider, A., Entezari, A., Vicedo-Cabrera, A.M., Zeka, A., Tobias, A., Nunes, B., Alahmad, B., Forsberg, B., Pan, S.-C., Íñiguez, C., Ameling, C., Valencia, C.D. la C., Åström, C., Houthuijs, D., Dung, D.V., Samoli, E., Mayvaneh, F., Sera, F., Carrasco-Escobar, G., Lei, Y., Orru, H., Kim, H., Holobaca, I.-H., Kyselý, J., Teixeira, J.P., Madureira, J., Katsouyanni, K., Hurtado-Díaz, M., Maasikmets, M., Ragettli, M.S., Hashizume, M., Stafoggia, M., Pascal, M., Scortichini, M., Coêlho, M. de S.Z.S., Ortega, N.V., Ryti, N.R.I., Scovronick, N., Matus, P., Goodman, P., Garland, R.M., Abrutzky, R., Garcia, S.O., Rao, S., Fratianni, S., Dang, T.N., Colistro, V., Huber, V., Lee, W., Seposo, X., Honda, Y., Guo, Y.L., Ye, T., Yu, W., Abramson, M.J., Samet, J.M., Li, S., 2021. Mortality risk attributable to wildfire-related PM2·5 pollution: a global time series study in 749 locations. Lancet Planet. Health 5, e579–e587. https://doi.org/10.1016/S2542-5196(21)00200-X.

Childs, M.L., Li, J., Wen, J., Heft-Neal, S., Driscoll, A., Wang, S., Gould, C.F., Qiu, M., Burney, J., Burke, M., 2022. Daily local-level estimates of ambient wildfire smoke $PM_{2.5}$ for the contiguous US. Environ. Sci. Technol. 56, 13607–13621. https://doi.org/10.1021/acs.est.2c02934.

Corwin, K.A., Corr, C.A., Burkhardt, J., Fischer, E.V., 2022. Smoke-driven changes in photosynthetically active radiation during the U.S. agricultural growing season. J. Geophys. Res. Atmos. 127, e2022JD037446 https://doi.org/10.1029/2022JD037446.

Dang, R., Jacob, D.J., Shah, V., Eastham, S.D., Fritz, T.M., Mickley, L.J., Liu, T., Wang, Y., Wang, J., 2022. Background nitrogen dioxide (NO_2) over the United States and its implications for satellite observations and trends: effects of nitrate photolysis, aircraft, and open fires. Atmos. Chem. Phys. 23, 6271–6284. https://doi.org/10.5194/acp-23-6271-2023.

Dennison, P.E., Brewer, S.C., Arnold, J.D., Moritz, M.A., 2014. Large wildfire trends in the western United States, 1984–2011. Geophys. Res. Lett. 41, 2928–2933. https://doi.org/10.1002/2014GL059576.

Eck, T.F., Holben, B.N., Reid, J.S., Dubovik, O., Smirnov, A., O'Neill, N.T., Slutsker, I., Kinne, S., 1999. Wavelength dependence of the optical depth of biomass burning, urban, and desert dust aerosols. J. Geophys. Res. Atmos. 104, 31333–31349. https://doi.org/10.1029/1999JD900923.

Eck, T.F., Holben, B.N., Giles, D.M., Slutsker, I., Sinyuk, A., Schafer, J.S., Smirnov, A., Sorokin, M., Reid, J.S., Sayer, A.M., Hsu, N.C., Shi, Y.R., Levy, R.C., Lyapustin, A., Rahman, M.A., Liew, S.-C., Salinas Cortijo, S.V., Li, T., Kalbermatter, D., Keong, K.L., Yuggotomo, M.E., Aditya, F., Mohamad, M., Mahmud, M., Chong, T.K., Lim, H.-S., Choon, Y.E., Deranadyan, G., Kusumaningtyas, S.D.A., Aldrian, E., 2019. AERONET remotely sensed measurements and retrievals of biomass burning aerosol optical properties during the 2015 Indonesian burning season. J. Geophys. Res. Atmos. 124, 4722–4740. https://doi.org/10.1029/2018JD030182.

Eck, T.F., Holben, B.N., Reid, J.S., Sinyuk, A., Giles, D.M., Arola, A., Slutsker, I., Schafer, J.S., Sorokin, M.G., Smirnov, A., LaRosa, A.D., Kraft, J., Reid, E.A., O'Neill, N.T., Welton, E.J., Menendez, A.R., 2023. The extreme forest fires in California/Oregon in 2020: aerosol optical and physical properties and comparisons of aged versus fresh smoke. Atmos. Environ. 305, 119798 https://doi.org/10.1016/j.atmosenv.2023.119798.

Eibedingil, I.G., Gill, T.E., Van Pelt, R.S., Tong, D.Q., 2021. Comparison of aerosol optical depth from MODIS product collection 6.1 and AERONET in the Western United States. Remote Sens. 13, 2316. https://doi.org/10.3390/rs13122316.

Ellis, T.M., Bowman, D.M.J.S., Jain, P., Flannigan, M.D., Williamson, G.J., 2022. Global increase in wildfire risk due to climate-driven declines in fuel moisture. Glob. Chang. Biol. 28, 1544–1559. https://doi.org/10.1111/gcb.16006.

Falah, S., Mhawish, A., Sorek-Hamer, M., Lyapustin, A.I., Kloog, I., Banerjee, T., Kizel, F., Broday, D.M., 2021. Impact of environmental attributes on the uncertainty in MAIAC/MODIS AOD retrievals: a comparative analysis. Atmos. Environ. 262, 118659 https://doi.org/10.1016/j.atmosenv.2021.118659.

Falah, S., Mhawish, A., Omar, A.H., Sorek-Hamer, M., Lyapustin, A.I., Banerjee, T., Kizel, F., Broday, D.M., 2022. Intercomparison of aerosol types reported as part of aerosol product retrieval over diverse geographic regions. Remote Sens. 14, 3667. https://doi.org/10.3390/rs14153667.

Fedschun, T., 2020. California Firefighters Battling Wildfire Face Gusty Winds, Smoke Dust Devils | Fox News.

Filonchyk, M., Peterson, M.P., Sun, D., 2022. Deterioration of air quality associated with the 2020 US wildfires. Sci. Total Environ. 826, 154103 https://doi.org/10.1016/j.scitotenv.2022.154103.

Geng, G., Murray, N.L., Tong, D., Fu, J.S., Hu, X., Lee, P., Meng, X., Chang, H.H., Liu, Y., 2018. Satellite-based daily PM2.5 estimates during fire seasons in Colorado. J. Geophys. Res. Atmos. 123, 8159–8171. https://doi.org/10.1029/2018JD028573.

Giles, D.M., Sinyuk, A., Sorokin, M.G., Schafer, J.S., Smirnov, A., Slutsker, I., Eck, T.F., Holben, B.N., Lewis, J.R., Campbell, J.R., Welton, E.J., Korkin, S.V., Lyapustin, A.I., 2019. Advancements in the Aerosol Robotic Network (AERONET) Version 3 database–automated near-real-time quality control algorithm with improved cloud screening for Sun photometer aerosol optical depth (AOD) measurements. Atmos. Meas. Tech. 12, 169–209. https://doi.org/10.5194/amt-12-169-2019.

González-Olalla, J.M., Powell, J.A., Brahney, J., 2024. Dust storms increase the tolerance of phytoplankton to thermal and pH changes. Glob. Chang. Biol. 30, e17055 https://doi.org/10.1111/gcb.17055.

Holben, B.N., Eck, T.F., Slutsker, I., Tanré, D., Buis, J.P., Setzer, A., Vermote, E., Reagan, J.A., Kaufman, Y.J., Nakajima, T., Lavenu, F., Jankowiak, I., Smirnov, A., 1998. AERONET—a federated instrument network and data archive for aerosol characterization. Remote Sens. Environ. 66, 1–16. https://doi.org/10.1016/S0034-4257(98)00031-5.

Holben, B.N., Kim, J., Sano, I., Mukai, S., Eck, T.F., Giles, D.M., Schafer, J.S., Sinyuk, A., Slutsker, I., Smirnov, A., Sorokin, M., Anderson, B.E., Che, H., Choi, M., Crawford, J. H., Ferrare, R.A., Garay, M.J., Jeong, U., Kim, M., Kim, W., Knox, N., Li, Z., Lim, H.S., Liu, Y., Maring, H., Nakata, M., Pickering, K.E., Piketh, S., Redemann, J., Reid, J.S., Salinas, S., Seo, S., Tan, F., Tripathi, S.N., Toon, O.B., Xiao, Q., 2018. An overview of mesoscale aerosol processes, comparisons, and validation studies from DRAGON networks. Atmos. Chem. Phys. 18, 655–671. https://doi.org/10.5194/acp-18-655-2018.

Holloway, T., Miller, D., Anenberg, S., Diao, M., Duncan, B., Fiore, A.M., Henze, D.K., Hess, J., Kinney, P.L., Liu, Y., Neu, J.L., O'Neill, S.M., Odman, M.T., Pierce, R.B., Russell, A.G., Tong, D., West, J.J., Zondlo, M.A., 2021. Annual Review of Biomedical Data Science, vol. 4, pp. 417–447. https://doi.org/10.1146/annurev-biodatasci-110920-093120.

Homer, C.G., Dewitz, J., Fry, J., Coan, M., Hossain, N., Larson, C., Herold, N., McKerrow, A.J., VanDriel, J.N., Wickham, J., 2007. Completion of the 2001 National Land Cover Database for the conterminous United States. Photogramm. Eng. Remote 73, 337.

Jaffe, D.A., O'Neill, S.M., Larkin, N.K., Holder, A.L., Peterson, D.L., Halofsky, J.E., Rappold, A.G., 2020. Wildfire and prescribed burning impacts on air quality in the United States. J. Air Waste Manage. Assoc. 70, 583–615. https://doi.org/10.1080/10962247.2020.1749731.

Jones, M.W., Abatzoglou, J.T., Veraverbeke, S., Andela, N., Lasslop, G., Forkel, M., Smith, A.J.P., Burton, C., Betts, R.A., van der Werf, G.R., Sitch, S., Canadell, J.G., Santín, C., Kolden, C., Doerr, S.H., Le Quéré, C., 2022. Global and regional trends and drivers of fire under climate change. Rev. Geophys. 60, e2020RG000726 https://doi.org/10.1029/2020RG000726.

Juliano, T.W., Jiménez, P.A., Kosović, B., Eidhammer, T., Thompson, G., Berg, L.K., Fast, J., Motley, A., Polidori, A., 2022. Smoke from 2020 United States wildfires responsible for substantial solar energy forecast errors. Environ. Res. Lett. 17, 034010 https://doi.org/10.1088/1748-9326/ac5143.

Keeley, J.E., Syphard, A.D., 2021. Large California wildfires: 2020 fires in historical context. Fire Ecol. 17, 22. https://doi.org/10.1186/s42408-021-00110-7.

Levy, M.E., Zhang, R., Khalizov, A.F., Zheng, J., Collins, D.R., Glen, C.R., Wang, Y., Yu, X.-Y., Luke, W., Jayne, J.T., Olaguer, E., 2013. Measurements of submicron aerosols in Houston, Texas during the 2009 SHARP field campaign. J. Geophys. Res. Atmos. 118, 10,518–10,534. https://doi.org/10.1002/jgrd.50785.

Li, L., Franklin, M., Girguis, M., Lurmann, F., Wu, J., Pavlovic, N., Breton, C., Gilliland, F., Habre, R., 2020a. Spatiotemporal imputation of MAIAC AOD using deep learning with downscaling. Remote Sens. Environ. 237, 111584 https://doi.org/10.1016/j.rse.2019.111584.

Li, L., Girguis, M., Lurmann, F., Pavlovic, N., McClure, C., Franklin, M., Wu, J., Oman, L. D., Breton, C., Gilliland, F., Habre, R., 2020b. Ensemble-based deep learning for estimating PM2.5 over California with multisource big data including wildfire smoke. Environ. Int. 145, 106143 https://doi.org/10.1016/j.envint.2020.106143.

Loría-Salazar, S.M., Holmes, H.A., Patrick Arnott, W., Barnard, J.C., Moosmüller, H., 2016. Evaluation of MODIS columnar aerosol retrievals using AERONET in semi-arid Nevada and California, U.S.A., during the summer of 2012. Atmos. Environ. 144, 345–360. https://doi.org/10.1016/j.atmosenv.2016.08.070.

Loría-Salazar, S.M., Sayer, A.M., Barnes, J., Huang, J., Flynn, C., Lareau, N., Lee, J., Lyapustin, A., Redemann, J., Welton, E.J., Wilkins, J.L., Holmes, H.A., 2021. Evaluation of novel NASA moderate resolution imaging spectroradiometer and visible infrared imaging radiometer suite aerosol products and assessment of smoke height boundary layer ratio during extreme smoke events in the Western USA. J. Geophys. Res. Atmos. 126, e2020JD034180 https://doi.org/10.1029/2020JD034180.

Lyapustin, A., Wang, Y., 2018. MODIS multi-angle implementation of atmospheric correction (MAIAC) data user's guide. Collection 6, version 2.0, NASA. https://lpdaac.usgs.gov/documents/110/MCD19_User_Guide_V6.pdf.

Lyapustin, A., Wang, Y., 2022. MODIS multi-angle implementation of atmospheric correction (MAIAC) data user's guide. Collection 6.1, version 3.1, NASA. https://lpdaac.usgs.gov/documents/1500/MCD19_User_Guide_V61.pdf.

Lyapustin, A., Korkin, S., Wang, Y., Quayle, B., Laszlo, I., 2012. Discrimination of biomass burning smoke and clouds in MAIAC algorithm. Atmos. Chem. Phys. 12, 9679–9686. https://doi.org/10.5194/acp-12-9679-2012.

Lyapustin, A., Wang, Y., Korkin, S., Huang, D., 2018. MODIS Collection 6 MAIAC algorithm. Atmos. Meas. Tech. 11, 5741–5765. https://doi.org/10.5194/amt-11-5741-2018.

Martins, V.S., Lyapustin, A., de Carvalho, L.a.S., Barbosa, C.C.F., Novo, E.M.L.M., 2017. Validation of high-resolution MAIAC aerosol product over South America. J. Geophys. Res. Atmos. 122, 7537–7559. https://doi.org/10.1002/2016JD026301.

McKendry, I.G., Christen, A., Lee, S.-C., Ferrara, M., Strawbridge, K.B., O'Neill, N., Black, A., 2019. Impacts of an intense wildfire smoke episode on surface radiation, energy and carbon fluxes in southwestern British Columbia, Canada. Atmos. Chem. Phys. 19, 835–846. https://doi.org/10.5194/acp-19-835-2019.

National Interagency Fire Center, 2020a. Wildfires and Acres | National Interagency Fire Center [WWW Document]. URL. https://www.nifc.gov/fire-information/statistics/wildfires (accessed 2.1.23).

National Interagency Fire Center, 2020b. Wildland fire summary and statistics annual report 2020. Retrieved from https://www.predictiveservices.nifc.gov/intelligence/2020_statssumm/annual_report_2020.pdf.

Nelson, M., 2020. Historic September 2020 fires & labor day windstorm. URL, FOX 12 Weather Blog. https://fox12weather.wordpress.com/historic-september-2020-fires-labor-day-windstorm/.

Nguyen, H.M., Wooster, M.J., 2020. Advances in the estimation of high Spatio-temporal resolution pan-African top-down biomass burning emissions made using geostationary fire radiative power (FRP) and MAIAC aerosol optical depth (AOD) data. Remote Sens. Environ. 248, 111971 https://doi.org/10.1016/j.rse.2020.111971.

O'Dell, K., Ford, B., Fischer, E.V., Pierce, J.R., 2019. Contribution of wildland-fire smoke to US $PM_{2.5}$ and its influence on recent trends. Environ. Sci. Technol. 53, 1797–1804. https://doi.org/10.1021/acs.est.8b05430.

O'Dell, K., Hornbrook, R.S., Permar, W., Levin, E.J.T., Garofalo, L.A., Apel, E.C., Blake, N.J., Jarnot, A., Pothier, M.A., Farmer, D.K., Hu, L., Campos, T., Ford, B., Pierce, J.R., Fischer, E.V., 2020. Hazardous air pollutants in fresh and aged Western US wildfire smoke and implications for long-term exposure. Environ. Sci. Technol. 54, 11838–11847. https://doi.org/10.1021/acs.est.0c04497.

Olson, N.E., Boaggio, K.L., Rice, R.B., Foley, K.M., LeDuc, S.D., 2023. Wildfires in the western United States are mobilizing PM2.5-associated nutrients and may be contributing to downwind cyanobacteria blooms. Environ Sci Process Impacts 25, 1049–1066. https://doi.org/10.1039/D3EM00042G.

Patel, K., 2020. Wildfire smoke shrouds the U.S. West [WWW Document]. URL, NASA Earth Obvervatory. https://earthobservatory.nasa.gov/images/147151/wildfire-smoke-shrouds-the-us-west.

Peterson, G.C.L., Prince, S.E., Rappold, A.G., 2021. Trends in fire danger and population exposure along the wildland–urban interface. Environ. Sci. Technol. 55, 16257–16265. https://doi.org/10.1021/acs.est.1c03835.

Petrenko, M., Ichoku, C., 2013. Coherent uncertainty analysis of aerosol measurements from multiple satellite sensors. Atmos. Chem. Phys. 13, 6777–6805. https://doi.org/10.5194/acp-13-6777-2013.

Petrenko, M., Ichoku, C., Leptoukh, G., 2012. Multi-sensor aerosol products sampling system (MAPSS). Atmos. Meas. Tech. 5, 913–926. https://doi.org/10.5194/amt-5-913-2012.

Ponette-González, A.G., Curran, L.M., Pittman, A.M., Carlson, K.M., Steele, B.G., Ratnasari, D., Mujiman, Weathers, K.C., 2016. Biomass burning drives atmospheric nutrient redistribution within forested peatlands in Borneo. Environ. Res. Lett. 11, 085003 https://doi.org/10.1088/1748-9326/11/8/085003.

Qin, W., Fang, H., Wang, L., Wei, J., Zhang, M., Su, X., Bilal, M., Liang, X., 2021. MODIS high-resolution MAIAC aerosol product: global validation and analysis. Atmos. Environ. 264, 118684 https://doi.org/10.1016/j.atmosenv.2021.118684.

Radeloff, V.C., Helmers, D.P., Kramer, H.A., Mockrin, M.H., Alexandre, P.M., Bar-Massada, A., Butsic, V., Hawbaker, T.J., Martinuzzi, S., Syphard, A.D., Stewart, S.I., 2018. Rapid growth of the US wildland-urban interface raises wildfire risk. Proc. Natl. Acad. Sci. 115, 3314–3319. https://doi.org/10.1073/pnas.1718850115.

Ranjan, A.K., Patra, A.K., Gorai, A.K., 2020. Effect of lockdown due to SARS COVID-19 on aerosol optical depth (AOD) over urban and mining regions in India. Sci. Total Environ. 745, 141024 https://doi.org/10.1016/j.scitotenv.2020.141024.

Roberts, G., Wooster, M.J., 2021. Global impact of landscape fire emissions on surface level PM2.5 concentrations, air quality exposure and population mortality. Atmos. Environ. 252, 118210 https://doi.org/10.1016/j.atmosenv.2021.118210.

Rogozovsky, I., Ansmann, A., Althausen, D., Heese, B., Engelmann, R., Hofer, J., Baars, H., Schechner, Y., Lyapustin, A., Chudnovsky, A., 2021. Impact of aerosol layering, complex aerosol mixing, and cloud coverage on high-resolution MAIAC aerosol optical depth measurements: fusion of lidar, AERONET, satellite, and ground-based measurements. Atmos. Environ. 247, 118163 https://doi.org/10.1016/j.atmosenv.2020.118163.

Rolph, G.D., Draxler, R.R., Stein, A.F., Taylor, A., Ruminski, M.G., Kondragunta, S., Zeng, J., Huang, H.-C., Manikin, G., McQueen, J.T., Davidson, P.M., 2009. Description and verification of the NOAA smoke forecasting system: the 2007 fire season. Weather Forecast. 24, 361–378. https://doi.org/10.1175/2008WAF2222165.1.

Safford, H.D., Paulson, A.K., Steel, Z.L., Young, D.J.N., Wayman, R.B., 2022. The 2020 California fire season: a year like no other, a return to the past or a harbinger of the future? Glob. Ecol. Biogeogr. 31, 2005–2025. https://doi.org/10.1111/geb.13498.

Schlosser, J.S., Braun, R.A., Bradley, T., Dadashazar, H., MacDonald, A.B., Aldhaif, A.A., Aghdam, M.A., Mardi, A.H., Xian, P., Sorooshian, A., 2017. Analysis of aerosol composition data for western United States wildfires between 2005 and 2015: dust emissions, chloride depletion, and most enhanced aerosol constituents. J. Geophys. Res. Atmos. 122, 8951–8966. https://doi.org/10.1002/2017JD026547.

Scordo, F., Chandra, S., Suenaga, E., Kelson, S.J., Culpepper, J., Scaff, L., Tromboni, F., Caldwell, T.J., Seitz, C., Fiorenza, J.E., Williamson, C.E., Sadro, S., Rose, K.C., Poulson, S.R., 2021. Smoke from regional wildfires alters lake ecology. Sci. Rep. 11, 10922 https://doi.org/10.1038/s41598-021-89926-6.

Sever, L., Alpert, P., Lyapustin, A., Wang, Y., Chudnovsky, A., 2017. An example of aerosol pattern variability over bright surface using high resolution MODIS MAIAC: the eastern and western areas of the Dead Sea and environs. Atmos. Environ. 165, 359–369. https://doi.org/10.1016/j.atmosenv.2017.06.047.

Shaylor, M., Brindley, H., Sellar, A., 2022. An evaluation of two decades of aerosol optical depth retrievals from MODIS over Australia. Remote Sens. 14, 2664. https://doi.org/10.3390/rs14112664.

Superczynski, S.D., Kondragunta, S., Lyapustin, A.I., 2017. Evaluation of the multi-angle implementation of atmospheric correction (MAIAC) aerosol algorithm through intercomparison with VIIRS aerosol products and AERONET. J. Geophys. Res. Atmos. 122, 3005–3022. https://doi.org/10.1002/2016JD025720.

Tao, M., Wang, Z., Tao, J., Chen, L., Wang, J., Hou, C., Wang, L., Xu, X., Zhu, H., 2017. How do aerosol properties affect the temporal variation of MODIS AOD bias in Eastern China? Remote Sens. 9, 800. https://doi.org/10.3390/rs9080800.

Tao, M., Wang, J., Li, R., Wang, Lili, Wang, Lunche, Wang, Z., Tao, J., Che, H., Chen, L., 2019. Performance of MODIS high-resolution MAIAC aerosol algorithm in China: characterization and limitation. Atmos. Environ. 213, 159–169. https://doi.org/10.1016/j.atmosenv.2019.06.004.

Tosca, M.G., Randerson, J.T., Zender, C.S., 2013. Global impact of smoke aerosols from landscape fires on climate and the Hadley circulation. Atmos. Chem. Phys. 13, 5227–5241. https://doi.org/10.5194/acp-13-5227-2013.

Vadrevu, K.P., Ellicott, E., Badarinath, K.V.S., Vermote, E., 2011. MODIS derived fire characteristics and aerosol optical depth variations during the agricultural residue burning season, north India. Environ. Pollut. 159, 1560–1569. https://doi.org/10.1016/j.envpol.2011.03.001.

Voiland, A., 2020. Historic fires devastate the U.S. Pacific Coast [WWW Document]. URL, NASA Earth Observatory. https://earthobservatory.nasa.gov/images/147277/historic-fires-devastate-the-us-pacific-coast.

Wagner, R., Schepanski, K., Klose, M., 2021. The dust emission potential of agricultural-like fires—theoretical estimates from two conceptually different dust emission parameterizations. J. Geophys. Res. Atmos. 126, e2020JD034355 https://doi.org/10.1029/2020JD034355.

Wen, J., Heft-Neal, S., Baylis, P., Boomhower, J., Burke, M., 2023. Quantifying fire-specific smoke exposure and health impacts. Proc. Natl. Acad. Sci. 120, e2309325120.

White, R., 2020. Dust storms, hazardous conditions forces closure of I-90 and several other highways in Eastern Washington | The Spokesman-Review. In: The Spokesman-Review.

Wickham, J., Stehman, S.V., Sorenson, D.G., Gass, L., Dewitz, J.A., 2021. Thematic accuracy assessment of the NLCD 2016 land cover for the conterminous United States. Remote Sens. Environ. 257, 112357 https://doi.org/10.1016/j.rse.2021.112357.

Wilmot, T.Y., Hallar, A.G., Lin, J.C., Mallia, D.V., 2021. Expanding number of Western US urban centers face declining summertime air quality due to enhanced wildland fire activity. Environ. Res. Lett. 16, 054036 https://doi.org/10.1088/1748-9326/abf966.

Wilmot, T.Y., Mallia, D.V., Hallar, A.G., Lin, J.C., 2022a. Wildfire plumes in the Western US are reaching greater heights and injecting more aerosols aloft as wildfire activity intensifies. Sci. Rep. 12, 12400 https://doi.org/10.1038/s41598-022-16607-3.

Wilmot, T.Y., Mallia, D.V., Hallar, A.G., Lin, J.C., 2022b. Wildfire activity is driving summertime air quality degradation across the western US: a model-based attribution to smoke source regions. Environ. Res. Lett. 17, 114014 https://doi.org/10.1088/1748-9326/ac9a5d.

Wooster, M.J., Roberts, G.J., Giglio, L., Roy, D.P., Freeborn, P.H., Boschetti, L., Justice, C., Ichoku, C., Schroeder, W., Davies, D., Smith, A.M.S., Setzer, A., Csiszar, I., Strydom, T., Frost, P., Zhang, T., Xu, W., de Jong, M.C., Johnston, J.M., Ellison, L., Vadrevu, K., Sparks, A.M., Nguyen, H., McCarty, J., Tanpipat, V., Schmidt, C., San-Miguel-Ayanz, J., 2021. Satellite remote sensing of active fires: history and current status, applications and future requirements. Remote Sens. Environ. 267, 112694 https://doi.org/10.1016/j.rse.2021.112694.

Yang, F., Wang, Y., Tao, J., Wang, Z., Fan, M., De Leeuw, G., Chen, L., 2018. Preliminary investigation of a new AHI aerosol optical depth (AOD) retrieval algorithm and evaluation with multiple source AOD measurements in China. Remote Sens. 10, 748. https://doi.org/10.3390/rs10050748.

Yang, X., Zhao, C., Yang, Y., Yan, X., Fan, H., 2021. Statistical aerosol properties associated with fire events from 2002 to 2019 and a case analysis in 2019 over Australia. Atmos. Chem. Phys. 21, 3833–3853. https://doi.org/10.5194/acp-21-3833-2021.

Zhang, Z., Wu, W., Fan, M., Wei, J., Tan, Y., Wang, Q., 2019. Evaluation of MAIAC aerosol retrievals over China. Atmos. Environ. 202, 8–16. https://doi.org/10.1016/j.atmosenv.2019.01.013.